PROCEEDINGS OF SCIENCE

Results from a low-threshold ultrahigh-energy neutrino search with the Askaryan Radio Array

Kaeli Hughes[a,*] **on behalf of the ARA Collaboration**

[a] *The University of Chicago, Chicago, IL, USA*

E-mail: kahughes@uchicago.edu

The Askaryan Radio Array (ARA) is an in-ice radio detector at the South Pole that targets radio emission from neutrino-induced particle cascades. Designed to detect neutrinos above 10 PeV, ARA has been taking data for over ten years and includes five independent stations. The newest ARA station is equipped with a phased array trigger, which lowers the trigger threshold compared to previous ARA stations and thus increases the neutrino sensitivity. In this contribution, we discuss the newest ARA analysis results from this phased array trigger and show a corresponding improvement in analysis efficiency, rejecting thermal backgrounds and providing vertex direction in the deep ice. We will also discuss the implications of this analysis for future radio-detection experiments.

9th International Workshop on Acoustic and Radio EeV Neutrino Detection Activities - ARENA2022
7-10 June 2022
Santiago de Compostela, Spain

*Speaker

PoS(ARENA2022)002

1. Introduction

Not much is known about the sources of the highest energy particles in the universe. While cosmic ray experiments have successfully measured the flux of cosmic rays above 10^{21} eV [1] [2], more investigation is necessary to determine which astrophysical objects must be producing these high energy particles.

Neutrinos are a natural candidate for answering these questions. As neutral particles that rarely interact, neutrinos can travel the length of the Universe without interacting, moving in a straight line from their sources. While IceCube has successfully measured the astrophysical neutrino flux up to a few PeV [3][4], there is reason to believe the neutrino flux extends to higher energies as well. These neutrinos above 10 PeV could be created directly in astrophysical sources [5] [6] or via interactions between cosmic rays and the cosmic microwave background [7].

In order to detect these rare events, detectors must be built to survey hundreds of square kilometers. Many detectors targeting the neutrino flux above 10 PeV are built to detect Askaryan radiation [8], in which coherent broadband radio emission is radiated from the particle shower following a neutrino interaction in a dense medium. Ice is a particularly advantageous medium for Askaryan radio detectors, as the long attenuation length makes it possible to survey a large volume of ice with minimal instrumentation.

In this work, we discuss one experiment, the Askaryan Radio Array (ARA), and results from a neutrino search conducted with one of its five stations. More details on this work are discussed in [9], and a summary of other recent work on ARA is discussed in [10].

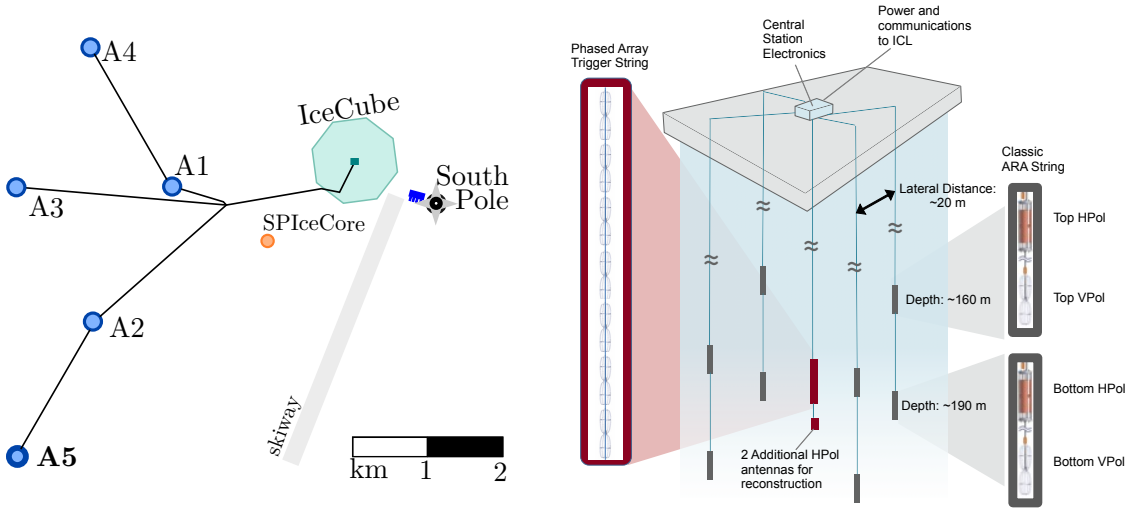

Figure 1: Left: A map of the currently deployed ARA stations at the South Pole, relative to known landmarks. Right: The layout of ARA Station 5, including the additional central string for the Phased Array antenna string.

2. The ARA Detector and the Phased Array Trigger

The ARA instrument, shown in Figure 1, consists of five independent stations, each separated by about 2 km from their neighboring stations. Each station includes four holes drilled to a maximum depth of 200 m, with four antennas distributed throughout the holes at varying depths and split between two polarizations to reconstruct the neutrino direction.

A typical ARA trigger is coincidence-based, requiring three antennas of the same polarization to exceed a threshold within a specific time window, limited by the time it takes for the radio signal to traverse a single station [11].

The most recently deployed ARA station, ARA station 5, includes an additional string of antennas that make up a beamforming trigger, as shown in Figure 1b, which is called the Phased Array instrument. In a beamforming trigger, signals are added together in pre-determined directions, called beams, before being sent through a power threshold trigger, causing the signals to add coherently if they are associated with a specific direction. Each of the 15 beams has its own trigger threshold that is adjusted in real-time to meet a global trigger requirement of 11 Hz. This method of triggering has a higher efficiency at lower signal-to-noise ratios (SNR, defined as $\frac{V_{pp}}{2\sigma_{noise}}$), which can be seen in Figure 4. This means that a beamforming trigger will trigger on more events than a typical ARA trigger, with particular improvement at the low energy range, at which smaller signals are typically produced.

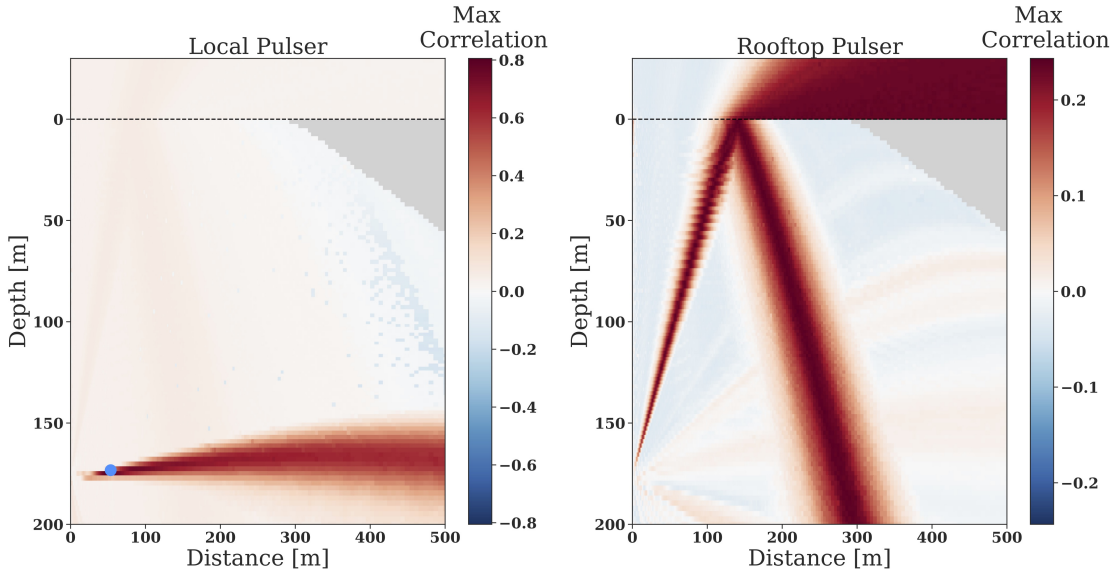

Figure 2: Two examples of R-z correlation maps for two types of calibration pulsers. Left: the local calibration pulser, with the true location of the pulse marked with a blue dot. Right: The surface pulser, with the true location about 4 km away on the roof of the IceCube Laboratory.

3. The Phased Array Analysis

This analysis included seven months of data from the Phased Array instrument during the calendar year 2019. While ARA Station 5 includes both a typical ARA trigger with four total

reconstruction strings and a beamforming trigger, this analysis focuses on only the central beamforming string and only uses the reconstruction strings minimally. Future analyses will take full advantage of the reconstruction strings, but this is considered outside the scope of this work.

We use the presample scaling method of blinding discussed in [12], where 10% of the total available data was unblinded and used to set cuts, and the remaining 90% was used to set the flux limit. The 10% sample was chosen by randomly selecting one out of every ten events. Additionally, one full 24-hour time window was unblinded to better learn about any behavior that impacted multiple events in a row.

In the following sections, the details of the analysis are discussed, along with the unblinding results.

3.1 R-z Correlation Mapping

The main tool used in this analysis was two dimensional reconstruction, evaluated in two directions: distance radially away from the phased array string (R), and depth relative to surface (z). Because the index of refraction of ice changes with depth, the incoming angle measured at the phased array itself corresponds to many pairs of R and z points within the ice. The correlation values shown on the map are calculated by adding up the signals on each channel as if they were coming from each point on the map, and calculating the average value across all channel pairs. Examples of two maps for different types of calibration pulser events are shown in Figure 2.

The brightest point on the correlation map corresponds to the point at which the signals best align, thus making it the most likely origin of the signal. For each event, a coherently summed waveform (CSW) is formed by taking the time delays associated with the brightest peak on the correlation map, and adding the signals together with the corresponding time delays. From this CSW and from the correlation map, a list of analysis variables can be built which describe various characteristics of the pulses in the dataset. Variables like SNR, the maximum correlation value, the impulsivity of the pulse, and the peak power are all used to discriminate between different classes of signal.

While the majority of events recorded by the phased array are expected to be thermal noise fluctuations, we also expect anthropogenic backgrounds, cosmic ray events, and potentially neutrino signals. The anthropogenic and cosmic ray events are the most challenging to remove, as they can look very similar to the expected impulsive neutrino signal. This analysis took a conservative approach and removed events that could have originated from the surface. Future analyses may have other methods of removing these anthropogenic or surface events, either through an azimuthal cut that points back towards the South Pole, or through a dedicated cosmic ray simulation that helps describe the expected background rate and zenith distribution. In later plots, the efficiency is presented both for this analysis, and what might be possible for a future analysis with a less conservative surface cut choice.

3.2 Fisher Discriminant modeling

After removing the events that pointed back towards the surface, as well as calibration pulser events and software trigger events, the remaining sample appeared to have the characteristics of thermal noise, with no obvious outlier events from other sources. To distinguish between thermal

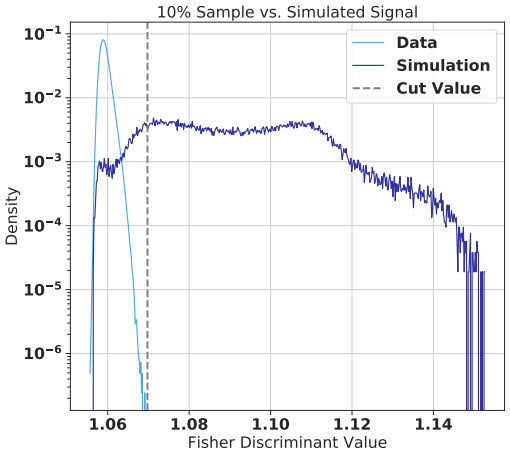

(a) Fisher Discriminant values for data vs. simulated neutrinos.

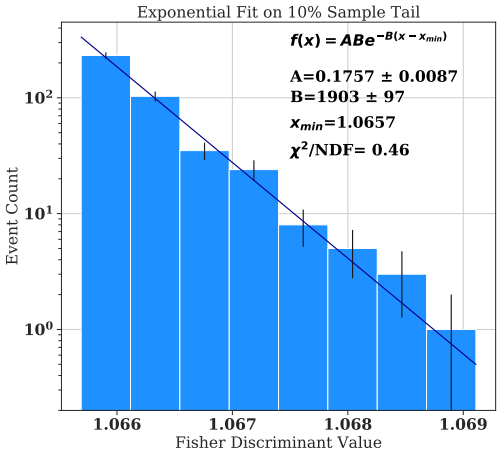

(b) The tail of the background distribution, including the exponential fit.

Figure 3: A comparison of the data and simulation distributions using the Fisher discriminant.

.

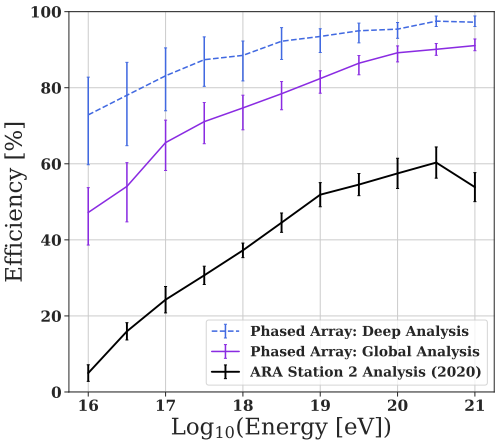

(a) The efficiency of this analysis vs. energy.

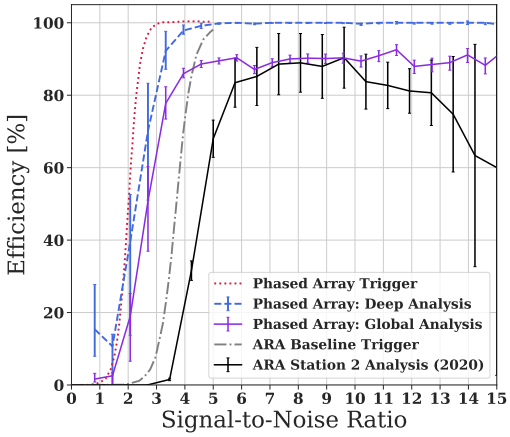

(b) The efficiency of this analysis as a function of SNR.

Figure 4: The efficiency of this analysis compared to the previous ARA analysis.

.

noise background events and neutrino signal events, a Fisher discriminant was trained against both the 10% sample from data and simulated neutrino events that were created using an optimistic cosmogenic model in the ARASim simulation package [13]. The Fisher discriminant was comprised of 19 total analysis variables, which are fully enumerated in [9]. The resulting Fisher values are linear combinations of each of the underlying analysis variables, projected along the axis which is most discriminatory between signal and background.

Cut Name	Events Remaining	Background Estimate	Signal Efficiency
None	18,651,857	N/A	100%
Deep Region Boundary	6,005,122	N/A	79.03%
Cal Pulser Gate Flag	4,423,436	N/A	99.98%
Cal Pulser Geometry Cut	4,411,686	0.009	99.64%
Software Trigger Cut	4,014,776	N/A	100%
Fisher Discriminant	0	$0.09^{+0.06}_{-0.04}$	86.58%
Total	0	$0.10^{+0.06}_{-0.04}$	68.16%

Table 1: Table of cuts, background estimates, and analysis efficiencies from the 10% sample in the deep region. For the Fisher Discriminant, the median background is reported, as are the 16th and 84th percentiles.

The distributions of the Fisher discriminant for both signal and background are shown in Figure 3. To determine the appropriate place for the cut, the tail of the data distribution is fit to an exponential so that the background level can be extrapolated to describe the 90% blinded dataset. Then, the location of the cut is optimized for the best expected sensitivity, with the sensitivity defined as the best 90% Feldman-Cousins upper limit. The final background estimate for each cut, as well as the total background estimate, is shown in Table 1.

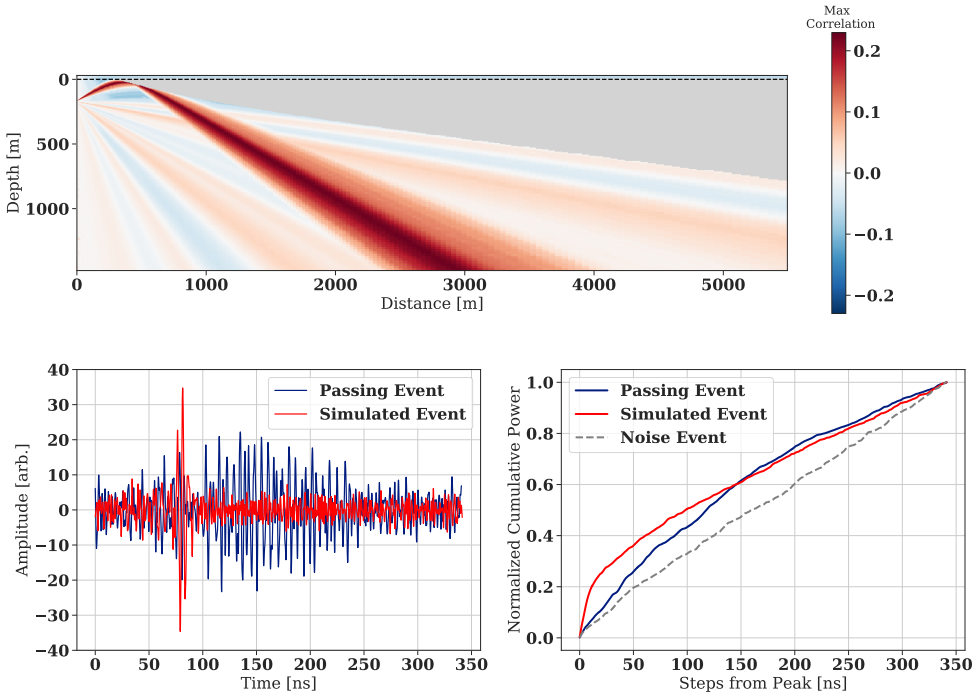

Figure 5: Top: the correlation map for the event that passed the analysis in the deep region. Bottom left: the CSW for the passing event, compared to a CSW from a simulated neutrino at a similar angle. Bottom right: The impulsivity measure for the passing event, compared to the simulated event and compared to noise.

3.3 Analysis Results

The analysis efficiency achieved in this analysis and shown in Figure 4 was significantly higher than previous ARA analyses, especially at the lowest energies. This is due to a combination of improved direction reconstruction, something possible for ARA Station 5 due to a better calibration and nearly identical antennas, and more sophisticated analysis techniques like the Fisher discriminant.

The analysis efficiency is also high when compared to the trigger efficiency of the beamforming trigger. It is clear from Figure 4 that the analysis efficiency of the beamforming trigger starts to turn on before the trigger efficiency curve for the ARA baseline trigger turns on, meaning that this analysis is efficient on events that a typical ARA station would not have triggered on. This is evidence that the benefits of the lower threshold of the beamforming trigger can be kept throughout an analysis.

After unblinding the analysis, one event passed in the deep region. This event is shown in Figure 5. This event independently triggered both the baseline ARA station and the beamforming trigger of the Phased Array, although the signal continues for a longer time than the expected neutrino signal. While the radio signal at the detector points above horizontal, the expected path curves away from the surface at a depth of around 30 m, making it too deep to be removed by the surface cut. The ARA baseline instrument reconstructs this event closer to horizontal, although the quality of this reconstruction is worse. It is possible that this event could be an impacting cosmic ray event that showers only after it hits the ice, or it could be a surface pulse traveling through a region of ice that is disallowed by the simple exponential model used to describe the changing index of refraction. We keep this event in our signal region when setting a limit, which can be seen in Figure 6. The projected limit includes a stricter surface cut.

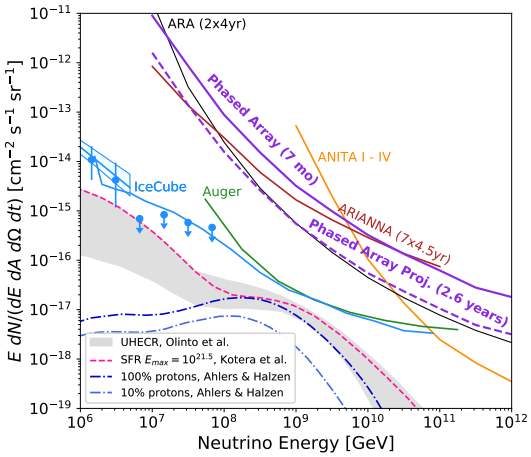

Figure 6: The limit from the phased array analysis, using six months of livetime, along with the projected sensitivity using a livetime of 2.6 years, corresponding to the data taken by the Phased Array through the end of 2021.

4. Conclusion

We continue to be optimistic about the use of beamforming triggers in the future. The expected limit of the Phased Array instrument improves quickly with increased livetime due to the highly efficient trigger and analysis of the Phased Array. While the Phased Array on its own would still take years to build up enough livetime to start approaching the expected astrophysical and cosmogenic neutrino models, other experiments can take advantage of this triggering technique at a larger scale.

In fact, other experiments like RNO-G and PUEO are already implementing this new type of trigger, and this work shows that that choice is well motivated.

It is also important to note that the passing event is suggestive of a new type of background that has not been modeled previously. Determining the origin of this event will be helpful to all in-ice detectors, regardless of their depth or design.

References

[1] A. Aab et al. Probing the origin of ultra-high-energy cosmic rays with neutrinos in the EeV energy range using the pierre auger observatory. *Journal of Cosmology and Astroparticle Physics*, 2019(10):022–022, oct 2019.

[2] T. Abu-Zayyad et al. The cosmic-ray energy spectrum observed with the surface detector of the telescope array experiment. *The Astrophysical Journal Letters*, 768(1):L1, apr 2013.

[3] M. G. Aartsen et al. Differential limit on the extremely-high-energy cosmic neutrino flux in the presence of astrophysical background from nine years of icecube data. *Phys. Rev. D*, 98:062003, Sep 2018.

[4] M. G. Aartsen et al. Observation and Characterization of a Cosmic Muon Neutrino Flux from the Northern Hemisphere using six years of IceCube data. *Astrophys. J.*, 833(1):3, 2016.

[5] Kohta Murase. *Active Galactic Nuclei as High-Energy Neutrino Sources*, pages 15–31. World Scientific, 2017.

[6] A. V. Olinto, K. Kotera, and D. Allard. Ultrahigh Energy Cosmic Rays and Neutrinos. *Nucl. Phys. Proc. Suppl.*, 217:231–236, 2011.

[7] K. Greisen. End to the Cosmic-Ray Spectrum? *Physical Review Letters*, 16:748–750, April 1966.

[8] G. A. Askar'yan. Excess negative charge of an electron-photon shower and its coherent radio emission. *Sov. Phys. JETP*, 14(2):441–443, 1962. [Zh. Eksp. Teor. Fiz.41,616(1961)].

[9] P. Allison et al. Low-threshold ultrahigh-energy neutrino search with the askaryan radio array. *Phys. Rev. D*, 105:122006, Jun 2022.

[10] S. Toscano and the ARA Collaboration. The Askaryan Radio Array: latest results and ongoing work. *In These proceedings*, 2022.

[11] P. Allison et al. Constraints on the diffuse flux of ultrahigh energy neutrinos from four years of askaryan radio array data in two stations. *Physical Review D*, 102(4), Aug 2020.

[12] J. R. Klein and A. Roodman. Blind analysis in nuclear and particle physics. *Ann. Rev. Nucl. Part. Sci.*, 55:141–163, 2005.

[13] K. Kotera, D. Allard, and A. V. Olinto. Cosmogenic Neutrinos: parameter space and detectabilty from PeV to ZeV. *JCAP*, 1010(10):013, 2010.